UCLA

Title

Cytoplasmic p53 couples oncogene-driven glucose metabolism to apoptosis and is a therapeutic target in glioblastoma

Permalink

https://escholarship.org/uc/item/423476tv

Authors

Mai, Wilson X
Gosa, Laura
Daniels, Veerle W
et al.

HHS Public Access

Author manuscript

Nat Med. Author manuscript; available in PMC 2018 April 09.

Cytoplasmic p53 couples oncogene-driven glucose metabolism to apoptosis and is a therapeutic target in glioblastoma

Wilson X. Mai[1], **Laura Gosa**[1], **Veerle W. Daniels**[6], **Lisa Ta**[1], **Jonathan E. Tsang**[1], **Brian Higgins**[8], **W. Blake Gilmore**[1], **Nicholas A. Bayley**[1], **Mitra Dehghan Harati**[5], **Jason T. Lee**[1,9], **William H. Yong**[5,9], **Harley I. Kornblum**[1,9], **Steven J. Bensinger**[4,9], **Paul S. Mischel**[7], **P. Nagesh Rao**[5], **Peter M. Clark**[1,9], **Timothy F. Cloughesy**[3,9], **Anthony Letai**[6], and **David A. Nathanson**[1,2,9]

[1]Department of Molecular and Medical Pharmacology, David Geffen UCLA School of Medicine, Los Angeles, California

[2]Ahmanson Translational Imaging Division, David Geffen UCLA School of Medicine, Los Angeles, California

[3]Department of Neurology, David Geffen UCLA School of Medicine, Los Angeles, California

[4]Department of Microbiology, Immunology, and Molecular Genetics, David Geffen UCLA School of Medicine, Los Angeles, California

[5]Department of Pathology, David Geffen UCLA School of Medicine, Los Angeles, California

[6]Department of Medical Oncology, Dana-Farber Cancer Institute, Boston, Massachusetts

[7]Ludwig Institute for Cancer Research, University of California San Diego, San Diego, California

[8]Pharma Research and Early Development, Roche Innovation Center, New York, NY

[9]Jonsson Comprehensive Cancer Center, David Geffen UCLA School of Medicine, Los Angeles, California

Abstract

Cross-talk among oncogenic signaling and metabolic pathways may create opportunities for novel therapeutic strategies in cancer. Here we show that acute inhibition of EGFR-driven glucose metabolism induces minimal cell death, yet lowers the apoptotic threshold in a subset of patient-derived glioblastoma (GBM) cells. Mechanistic studies revealed that, following attenuated glucose consumption, Bcl-xL blocks cytoplasmic p53 from triggering intrinsic apoptosis. Consequently, pharmacological stabilization of p53 with the brain-penetrant small molecule, Idasanutlin, in combination with targeting EGFR-driven glucose metabolism promoted synthetic lethality in

orthotopic xenograft models. Notably, neither inhibition of EGFR signaling, nor genetic analysis of *EGFR*, was sufficient to predict sensitivity to this new therapeutic combination. Conversely, rapid changes in ^{18}F-fluorodeoxyglucose (^{18}F-FDG) uptake using non-invasive positron emission tomography was an effective predictive biomarker of response in vivo. Together, these studies identify a critical link between oncogene signaling, glucose metabolism, and cytoplasmic p53, which could be exploited for combination therapy in GBM and potentially, other malignancies.

Introduction

Molecularly targeted therapies have revolutionized cancer treatment and paved the path for modern precision medicine. However, despite well-defined actionable genetic alterations[1], targeted drugs have failed in glioblastoma (GBM) patients. This is in large part due to insufficient brain penetration of most targeted agents to levels necessary for tumor kill[2]; this insufficient abundance in the target tissue may induce the development of adaptive mechanisms that drive drug resistance[3]. While therapeutic combinations that target both the primary genetic lesion and the compensatory signaling pathway(s) that promote resistance are appealing, these combination therapy strategies have been hampered by toxicities, requiring subthreshold dosing of each drug[4,5]. Owing to the dismal prognosis for GBM patients, and the poor efficacy of conventional approaches, new therapeutic strategies are critically needed.

An alternative therapeutic approach—synthetic lethality—targets an oncogenic driver to modify an important functional property for tumorigenesis, rendering cells vulnerable to an orthogonal second hit[6]. This strategy may be particularly attractive when the oncogene-regulated functional network(s) modulate tumor cell death pathways. In a notable example, oncogenic signaling drives glucose metabolism to suppress the intrinsic (or mitochondria-dependent) apoptotic pathway and prevent cell death[7,8]. Consequently, inhibition of oncogenic drivers with targeted therapies can trigger the intrinsic apoptotic machinery as a direct consequence of attenuated glucose consumption[7]. The intertwined nature of these tumorigenic pathways may present therapeutic opportunities for rational combination treatments, but this has yet to be investigated.

Previous work demonstrated that the epidermal growth factor receptor (EGFR) – mutated and/or amplified in ~60% of GBM patients [9] – regulates glucose metabolism[10]. Whether targeting EGFR-driven glucose utilization alters the dynamics of the intrinsic apoptotic machinery in cancer is unknown. Here we hypothesized that a deeper understanding of this relationship will reveal pharmacological vulnerabilities for enhanced tumor killing in GBM.

Results

EGFR inhibitor metabolic responders and non-responders

We first characterized the changes in glucose uptake induced by acute EGFR inhibition across 19 patient-derived GBM cell lines. The cells were cultured in supplemented serum-free medium as gliomaspheres which, in contrast to serum-based culture conditions, preserve many of the molecular features of patient tumors[11,12]. Treatment with the EGFR

tyrosine kinase inhibitor erlotinib revealed a subset of GBMs whose radio-labeled glucose uptake (^{18}F-FDG) was significantly attenuated, hereafter termed "metabolic responders" (Fig. 1a and Supplementary Fig. 1a). Silencing of *EGFR* using siRNA confirmed that the reduction in glucose uptake was not due to off-target effects of erlotinib (Supplementary Fig. 1b, c). Reduced ^{18}F-FDG uptake was associated with, as determined from a randomly selected cohort of metabolic responders, decreased lactate secretion, glucose consumption, and extracellular acidification rate (ECAR), yet glutamine levels remained unchanged (Fig. 1b and Supplementary Fig. 1d-g). Suppressed glucose utilization also correlated with a decrease in RAS-MAPK and PI3K-AKT-mTOR signaling – each of which can regulate glucose metabolism in GBM and other cancers [10,13,14] (Supplementary Fig. 2a).

In contrast, no "non-responder" GBMs (Fig. 1a and Supplementary Fig. 1b, c), showed reduced glucose consumption, lactate secretion, or ECAR despite robust inhibition of EGFR activity (Fig. 1b and Supplementary Fig. 1d-g) (Supplementary Fig. 2b). Moreover, RAS-MAPK and PI3K-AKT-mTOR signaling were unchanged in nearly all metabolic non-responders (Supplementary Fig. 2b). Notably, while all metabolic responders had alterations in *EGFR* (mutation and/or amplification, polysomy), 6 GBM lines without a metabolic response also contained *EGFR* mutations and/or copy number gains (Supplementary Fig. 3a, b). Taken together, these data illustrate two key points. First, acute inhibition of EGFR rapidly attenuates glucose utilization in a subset of primary GBM cells, and second, genetic alterations in *EGFR* could not alone predict which GBMs have a metabolic response to EGFR inhibition.

Metabolic responders are primed for apoptosis

Perturbations in glucose metabolism can induce the expression of pro-apoptotic factors and promote intrinsic apoptosis[15], leading us to posit that reduced glucose uptake in response to EGFR inhibition would stimulate the intrinsic apoptotic pathway. Indeed, acute erlotinib treatment enhanced the expression of the pro-apoptotic BH3-only proteins, BIM and PUMA, only in the metabolic responder cultures (Supplementary Fig. 4a). However, annexin V staining revealed that the metabolic responders had only modest (~17% cells annexin V positive), albeit significantly higher, apoptosis compared with non-responders (~3% cells annexin V positive), following 72 hours of erlotinib exposure (Fig. 1c).

The relatively low level of apoptosis in metabolic responder GBMs, despite pronounced induction of pro-apoptotic factors, led us to ask if perturbing glucose uptake with erlotinib simply "primes" GBM cells for apoptosis; thus increasing the propensity for apoptosis without inducing considerable cell death[16]. The induction of a primed apoptotic state, or a shift in the death threshold, can be measured by BH3 profiling; which, is conducted via exposing the mitochondria of drug-treated cells to synthetic pro-apoptotic BH3 peptides (e.g., BIM, BID, and/or PUMA) and then quantifying the changes in mitochondria potential – via cytochrome *c* release – to precisely determine the proximity of cells to intrinsic apoptosis[17]. Accordingly, we treated both metabolic responders and non-responders for 24 hours and performed BH3 profiling using multiple BH3 peptides across various concentrations (Supplementary Fig. 4b). We observed heightened apoptotic priming - as determined by the change in cytochrome *c* release relative to vehicle - in the metabolic

responders with erlotinib treatment (Fig. 1d). Importantly, priming in the metabolic responders was significantly higher than priming in the non-responders (Fig. 1d), supporting the premise that attenuated glucose uptake with EGFR inhibition triggers apoptotic priming in GBM.

We reasoned that if reduced glucose uptake is required for apoptotic priming with targeting EGFR, rescuing glucose consumption should mitigate these effects. Given that EGFR inhibition can abrogate the expression/localization of glucose transporters 1 (GLUT1) and 3 (GLUT3) (Supplemental Fig. 5a)[10], we ectopically expressed both GLUT1 and GLUT3 in two metabolic responder GBMs (HK301 and GBM39) to sustain glucose flux under erlotinib treatment. Enforced expression of GLUT1 and GLUT3 (GLUT1/3) rescued erlotinib-mediated attenuation of glucose consumption and lactate secretion in both cell lines (Fig. 1e and Supplementary Fig. 5b - d) and, importantly, markedly suppressed apoptotic priming in response to EGFR inhibition (Fig. 1f). Collectively, these data demonstrate that erlotinib-mediated inhibition of glucose metabolism, although insufficient to induce meaningful cell death, lowers the apoptotic threshold potentially rendering GBM cells vulnerable to agents that exploit this primed state.

Cytoplasmic p53 is required for apoptotic priming

Next, we investigated the mechanism by which GBMs become primed for apoptosis after treatment with erlotinib. In cells that are primed, the anti-apoptotic Bcl-2 family proteins (e.g. Bcl-2, Bcl-xL, Mcl-1) are largely loaded with pro-apoptotic BH3 proteins (e.g., BIM, BID, PUMA, BAD, NOXA, HRK); consequently, cells are dependent on these interactions for survival[16]. The tumor suppressor protein, p53, upregulates expression of pro-apoptotic proteins that subsequently need to be sequestered by anti-apoptotic Bcl-2 proteins to prevent cell death[18]. To examine whether p53 is required for erlotinib-induced priming, we abrogated p53 expression in two metabolic responders (HK301 and HK336) using CRISPR-Cas9 targeting *TP53*; the resulting cells are hereafter referred to as p53KO (Fig. 2a). While the change in glucose uptake with erlotinib was unaffected in p53KO cells (Supplementary Fig. 6a), BH3 profiling revealed p53KO nearly abolished erlotinib-induced apoptotic priming (Fig. 2b)

As transcription of p53 target genes has been shown to be enhanced under glucose limitation[15,19,20], we tested whether p53-mediated transcription was induced by EGFR inhibition. However, erlotinib neither increased the expression of p53-regulated genes (e.g., *p21*, *MDM2*, *PIG3*, *TIGAR*) (Supplementary Fig. 6b), nor induced p53-luciferase reporter activity in HK301 metabolic responder cells (Supplementary Fig. 6c). These data indicate that while p53 is required for priming with EGFR inhibition, its transcriptional activity may not be necessary.

In addition to p53's well-described nuclear functions, p53 can localize in the cytoplasm where it can directly engage the intrinsic apoptotic machinery via interactions with pro-apoptotic and/or anti-apoptotic Bcl-2 family members[21,22]. To evaluate whether cytoplasmic p53 is important for apoptotic priming with erlotinib, we stably introduced a p53 mutant with a defective nuclear localization signal (p53cyto)[23] into HK301 and HK336 p53KO gliomaspheres. As expected, p53cyto was expressed (Fig. 2c and Supplemental Fig. 6d),

restricted to the cytoplasm (Fig. 2d and Supplemental Fig. 6e) and had no transcriptional activity (Fig. 2e and Supplemental Fig. 2f). Conversely, reconstitution of wild-type p53 (p53^{wt}) in HK301 and HK336 p53KO cells displayed similar localization as parental cells and rescued transcription of p53-regulated genes (Fig. 2c - e and Supplemental Fig. 6e - g). Stable introduction of p53^{cyto} significantly restored priming with erlotinib in both HK301 and HK336 p53KO cells to levels comparable to p53^{wt} (Fig. 2f and Supplemental Fig. 6g), indicating that the cytoplasmic function of p53 is required for erlotinib-mediated priming. In support of this conclusion, introduction of a transcriptionally active (Fig. 2g), yet nuclear-confined p53 mutant (p53^{NES}) into HK301 p53KO cells failed to induce erlotinib-mediated apoptotic priming (Fig. 2g, h and Supplemental Fig. 6h). Finally, pharmacological inhibition of cytoplasmic p53 activity with pifithrin-μ (PFTμ)[24] markedly reduced priming with erlotinib (Supplementary Fig. 6i). Collectively, these results show that cytoplasmic p53 engages the intrinsic apoptotic machinery following treatment with erlotinib in GBM metabolic responder samples.

Prior work demonstrated that *TP53* mutations detected in human tumors – specifically those in the DNA binding domain – have diminished cytoplasmic functions in addition to transactivation deficiencies[22,25]. Thus, we asked whether stable expression of two of these "hotspot" p53 mutants, R175H or R273H, in HK301 p53KO would have reduced EGFRi-mediated apoptotic priming (Supplementary Fig. 6h). As expected, both mutants lacked transcriptional capabilities (Fig. 2g) and, consistent with reduced cytoplasmic activity, were incapable of priming with erlotinib (Fig. 2h). Therefore, in line with previous findings, oncogenic mutations in the DNA binding domain of p53 result in "dual hits"[26], whereby both transactivation and cytoplasmic functions are abrogated – the latter having implications for apoptotic priming with EGFR inhibition.

Inhibition of glucose uptake creates therapeutic vulnerability

Bcl-xL can sequester cytoplasmic p53 and prevent p53-mediated apoptosis; thus creating a primed apoptotic state and a dependency on Bcl-xL for survival[27]. Indeed, BH3 profiling revealed a reliance on Bcl-xL to block apoptosis in erlotinib metabolic responders (Supplementary Fig. 7a). Therefore, we hypothesized that attenuated glucose consumption with EGFR inhibition may result in the sequestration of cytoplasmic p53 by Bcl-xL. To investigate this, we performed co-immunoprecipitations to examine the dynamics of p53-Bcl-xL interactions in response to erlotinib in both responders (*n*=2) and non-responders (*n*=2). Importantly, we observed increased Bcl-xL and p53 complex formation with erlotinib treatment in metabolic responders (Fig. 3a) but not in non-responders (Fig. 3b). This suggests that inhibition of EGFR-dependent glucose consumption results in sequestration of p53 by Bcl-xL. Consistent with this interpretation, ectopic expression of GLUT1/3, which rescues the erlotinib-mediated reduction in glucose uptake and apoptotic priming, prevented the association of p53 with Bcl-xL (Fig. 3c and Supplementary Fig. 7b). These findings strongly indicate that erlotinib-mediated inhibition of glucose uptake primes GBM cells for apoptosis by promoting an interaction between cytoplasmic p53 and Bcl-xL.

Disruption of the p53 and Bcl-xL complex can "free" cytoplasmic p53 to stimulate intrinsic apoptosis[27]. Once we detected increased binding between Bcl-xL and p53 in metabolic

responders in response to erlotinib, we asked whether the liberation of p53 from Bcl-xL elicits apoptosis. To test this, we treated a metabolic responder (HK301) with erlotinib and the specific Bcl-xL inhibitor, WEHI-539[28]. The addition of WEHI-539 released p53 from Bcl-xL under erlotinib treatment (Fig. 3d), leading to synthetic lethality in three metabolic responders (HK301, GBM39, HK336) (Fig. 3e and Supplementary Fig. 7c). Notably, cytoplasmic p53 was sufficient for caspase-dependent apoptosis elicited by the drug combination (Supplementary Fig. 7c, e). However, WEHI-539 did not enhance apoptosis in a non-responder (HK393) treated with erlotinib, suggesting that attenuation of glucose uptake with EGFR inhibition, and subsequent association between p53 and Bcl-xL, is necessary to lower the apoptotic threshold and generate a dependence on Bcl-xL for survival (Fig. 3e). In support of this, enforced expression of GLUT1/3 significantly mitigated cell death with the drug combination (Fig. 3f and Supplementary Fig. 7d). Together, these observations indicate that Bcl-xL blocks GBM cell death in response to erlotinib-mediated inhibition of glucose metabolism by sequestering cytoplasmic p53 (Fig. 3g).

Combination treatment efficacy in metabolic responders

Our mechanistic studies reveal a potential therapeutic opportunity in EGFR-driven GBMs that will be dependent on functional p53. While the p53 signaling axis is one of the three core pathways altered in GBM[1,29], analysis of the TCGA GBM dataset demonstrated that *TP53* mutations are mutually exclusive with alterations in *EGFR* (Fig. 4a, b). Conversely, in most patients with *EGFR* mutations or gains, there are co-occurring alterations that can lead to suppressed p53 activity; this includes amplification of *MDM2* and/or deletions in the negative regulator of MDM2, p14 ARF, at the *CDKN2A* locus [30,31] (Fig. 4a, b). Given these relationships, and the requirement of p53 for priming under erlotinib-attenuated glucose uptake, we hypothesized that stabilization of p53 via MDM2 inhibition may have similar therapeutic effects to Bcl-xL antagonism. Using nutlin – an extensively characterized inhibitor of MDM2[32] – we noted synthetic lethality when paired with erlotinib in a metabolic responder gliomasphere. Greater than 90% of HK301 cells underwent apoptosis with combined erlotinib and nutlin (Fig. 4c). In contrast, we observed no synergy between these drugs in a metabolic non-responder (HK393, Fig. 4c). We then tested this combination across our panel of primary GBM cells (all p53 wild-type) and found synthetic lethality only in GBMs with a metabolic response to erlotinib, albeit less so in HK423 and HK296 metabolic responders (Fig. 4d and Supplementary Fig. 8a)[33]. Silencing of *EGFR* in combination with nutlin also showed selective synergy for metabolic responder cells, suggesting that the effects of the drug combination were not due to any off-target effects of erlotinib (Supplemental Fig. 8b). Importantly, enforced expression of GLUT1/3 significantly reduced molecular markers of intrinsic apoptosis – including BAX oligomerization, and cytochrome *c* release - as well as cell death with combined erlotinib and nutlin (Fig. 4e and Supplementary Fig. 8c), supporting the concept that attenuated glucose metabolism with EGFR inhibition is required for the synthetic lethality of the drug combination.

We next investigated the role of p53 in eliciting cell death to combined erlotinib and nutlin. As expected, p53KO in two erlotinib metabolic responders (HK301 and HK336) abolished sensitivity to the drug combination (Fig. 4f and Supplementary Fig. 8g). Likewise, ectopic expression of Bcl-xL markedly suppressed cell death with combined treatment, consistent

with a critical function for Bcl-xL in antagonizing p53-mediated apoptosis (Supplementary Fig. 8d). Moreover, similar to our results with Bcl-xL inhibition (e.g., WEHI-539), the addition of nutlin liberated p53 from Bcl-xL under erlotinib treatment (Fig. 4g). These data are in agreement with prior observations that p53 stabilization can stimulate cytoplasmic p53-mediated apoptosis[27,34]. In support of the suggestion that cytoplasmic p53 activity is required for the synergy of erlotinib and nutlin in metabolic responders, blocking cytoplasmic p53 activity with PFTµ significantly mitigated apoptosis elicited with the combination (Supplementary Fig. 8e), while HK301 cells containing the nuclear-confined p53 mutant, p53[NES], were incapable of enhanced cell death with the drug combination (Supplementary Fig. 8f). Finally, cells expressing the cancer "hotspot" p53 mutants, R175H and R273H, which have both transactivation and cytoplasmic deficiencies, were completely insensitive to the erlotinib and nutlin combination (Supplementary Fig. 8f).

It is noteworthy that while cytoplasmic p53 is absolutely required to promote cell death with combined erlotinib and nutlin, we observed in some instances that both the transcription-dependent (i.e. nuclear) and independent functions of p53 (i.e. cytoplasmic) are needed for optimal execution of synergistic apoptosis with nutlin (Supplementary Fig. 8g). These results are consistent with reports that the cytoplasmic functions of p53 can alone execute intrinsic apoptosis[34,35], whereas, in other contexts, may also require its nuclear functions to facilitate cytoplasmic p53 mediated cell kill[27]. Collectively, our results show that combined targeting of EGFR-driven glucose metabolism and p53 can induce marked synthetic lethality in primary GBM; which is dependent on the cytoplasmic functions of p53.

Priming metabolic non-responders for apoptosis

Our data has led us to propose a model where inhibition of EGFR-driven glucose metabolism primes the apoptotic machinery, resulting in synergy with pro-apoptotic stimuli such as p53 activation. A logical prediction of this model is that direct targeting of glucose metabolism should phenocopy the effects of EGFR inhibition. Consistent with this, addition of the glucose metabolic inhibitor 2-deoxyglucose (2DG) stimulated apoptotic priming, binding of p53 to Bcl-xL, and synthetic lethality with nutlin in HK301 metabolic responder cells. (Supplementary Fig. 9a, b, d). In contrast, inhibition of oxidative phosphorylation with oligomycin (complex V/ATP synthase) or rotenone (complex I) did not synergize with nutlin treatment in HK301 gliomaspheres (Supplementary Fig. 9c, d). Thus, reduced glucose metabolic flux alone, but not oxidative metabolism, appears to be sufficient for synergistic sensitivity to p53 activation.

This prompted us to consider whether modulating glucose consumption in non-responders results in a similar p53-dependent vulnerability. To investigate this, we tested whether direct inhibition of glucose uptake, with 2DG, or through targeting PI3K – a well characterized driver of glucose metabolism[36] - elicits apoptotic priming in two erlotinib metabolic non-responders (Fig. 5a). In contrast to erlotinib treatment, acute inhibition of PI3K with pictilisib abrogated PI3K-AKT-mTOR signaling (Supplementary Fig. 9e), and significantly reduced ^{18}F-FDG uptake in HK393 and HK254 cells (Fig. 5b). The decrease in glucose consumption with pictilisib was associated with significantly higher apoptotic priming; 2DG treatment induced similar effects (Fig. 5b, c). Therefore, erlotinib metabolic non-responders

can be primed for apoptosis following inhibition of glucose uptake. Importantly, CRISPR/CAS-9 targeting of p53 in HK393 cells significantly suppressed priming mediated by 2DG or pictilisib. (Fig. 5d). Moreover, p53-dependent priming was associated with heightened Bcl-xL and p53 binding, indicative of sequestration of p53 by Bcl-xL to block apoptosis (Fig. 5e and Supplementary Fig. 9f). In agreement with this interpretation, combining 2DG or pictilisib with nutlin caused significant, p53-dependent synthetic lethality in erlotinib non-responder cells (Fig. 5f, g). Taken together, these data demonstrate that acute inhibition of glucose metabolism, either directly or with targeted therapy, promotes p53-dependent apoptotic priming in GBM which creates a targetable vulnerability.

A non-invasive biomarker for combination treatment *in vivo*

Our results in cell culture show that combined targeting of oncogene-driven glucose metabolism and p53 has synergistic activity in primary GBM. This led us to investigate whether this approach could be effective in orthotopic GBM xenograft models. For these studies, we used the MDM2 inhibitor, Idasanutlin, which is currently in clinical trials for many malignancies[37]. Given the uncertainty of CNS penetration of Idasanutlin, we first demonstrated that Idasanutlin can accumulate in the brains of mice with a completely intact blood-brain-barrier (~35% relative to plasma levels) and stabilizes p53 in orthotopic tumor-bearing mice (Supplementary Fig. 10a, b).

Next, as perturbations in glucose metabolism with oncogene inhibition are required for synergistic sensitivity to p53 activation, we hypothesized that rapid attenuation in glucose uptake *in vivo* following erlotinib administration – as measured by ^{18}F-FDG PET – could serve as a non-invasive predictive biomarker for therapeutic efficacy of combined erlotinib and Idasanutlin treatment (Fig. 6a). We observed, in orthotopic xenografts of a metabolic responder gliomasphere (GBM39), that acute erlotinib treatment (75 mg/kg) rapidly reduced ^{18}F-FDG uptake (15 hours post erlotinib administration, see Materials and Methods) (Fig. 6b and Supplementary Fig. 10c). In separate groups of mice, we tested the individual drugs and the combination of daily erlotinib (75 mg/kg) and Idasanutlin (50 mg/kg) treatment for up to 25 days. The drug combination was tolerable over the treatment period; we noted a ~10% decrease in body weight, which was comparable to erlotinib treatment alone (Supplementary Fig. 10d). Relative to single agent controls, combined erlotinib and Idasanutlin demonstrated synergistic growth inhibition – as determined by secreted *gaussia* luciferase[38] - in GBM39 intracranial tumor-bearing mice (Fig. 6c and). In contrast, orthotopic xenografts of a non-metabolic responder (HK393) showed no changes in ^{18}F-FDG uptake with acute erlotinib (Fig. 6d and Supplementary Fig. 10c), nor synergistic activity with the erlotinib and Idasanutlin combination (Fig. 6e). Thus, non-invasive ^{18}F-FDG PET, used to measure rapid changes in glucose uptake with EGFR inhibition, was effective in predicting subsequent synergistic sensitivity to combined erlotinib and Idasanutlin

Finally, we evaluated the effects of the drug combination on overall survival in orthotopic xenografts of either two erlotinib metabolic responders (GBM39 and HK336) or two non-responders (HK393 and GS025). All tumors were p53 wild-type (Supplemental Fig. 3a). Following evidence of tumor growth (as determined by *gaussia* luciferase), mice were

treated with vehicle, erlotinib, Idasanutlin, or the combination for up to 25 days and then release of therapy; the short-term treatment due to limited quantities of Idasanutlin for these studies. Despite all tumors having genetic alterations in *EGFR* (e.g., mutation and/or amplification, polysomy), the drug combination led to a pronounced increase in survival only in animals bearing erlotinib metabolic responder GBM tumors (Fig. 6f-i). Taken together, these data show that combined targeting of EGFR and p53 synergistically inhibits growth and prolongs survival in a subset of p53 wild-type GBM orthotopic xenografts, and that ^{18}F-FDG PET is a non-invasive predictive biomarker of sensitivity to this new combination therapeutic strategy.

Discussion

Here we found that acute EGFR inhibition rapidly reduces glucose utilization in a subset of patient-derived GBMs. As a consequence to this altered metabolic state, unexpectedly, cells become primed for apoptosis via the cytoplasmic functions of p53. Accordingly, pharmacological p53 stabilization – with a novel brain-penetrant small molecule - was synthetically lethal with inhibition of EGFR-driven glucose uptake in primary orthotopic GBM models. While these preclinical systems do not fully recapitulate the features of human GBM - consisting of an active immune system, pseudopalisading necrosis, and microvasculature proliferation - our results provide a proof of concept that deploying targeted agents to perturb and exploit altered tumor metabolism could be an effective therapeutic strategy in GBM.

The majority of studies suggest that the apoptotic functions of p53 are primarily exerted through its transcriptional activity. However, recent work supports the suggestion that the non-transcriptional functions of p53 can have a critical role in triggering intrinsic apoptosis[26]. Our results provide, to the best of our knowledge, the first demonstration that cytoplasmic p53 couples oncogenic signaling to intrinsic apoptosis; which in this case is dependent on alterations in glucose utilization. However, it is remains unknown the metabolic pathway(s) downstream of glucose uptake that is responsible for this effect. The observation that direct inhibition of oxidative phosphorylation does not synergize with p53 activation suggests that oxidation of glucose or other metabolites (e.g., glutamine) is not required (Supplementary Fig. 9c, d). Glucose can feed into many metabolic pathways including those for anabolic processes (e.g., lipids, nucleotides, amino acids), energetics, and enzyme function (e.g., glycosylation, acetylation). Thus, attenuated glucose consumption may affect multiple pathways to induce sufficient metabolic stress[39] and/or reduced donor metabolic substrates[40,41] to stimulate the cytoplasmic functions of p53. Future studies are required to specifically define these metabolic nodes that render GBM cells exquisitely susceptible to cytoplasmic p53-mediated apoptosis. This could reveal analogous therapeutic vulnerabilities to exploit GBM tumors for p53-dependent cell death.

More work is also needed to understand precisely how cytoplasmic p53 triggers intrinsic apoptosis in GBM cells. Considerable evidence indicates that cytoplasmic p53 possesses similar functionality as pro-apoptotic BH3 proteins, where it can activate the pro-apoptotic effectors BAK[22,42] or BAX directly[21] and/or indirectly via neutralizing anti-apoptotic Bcl2 proteins[22]. Our results support this role for cytoplasmic p53 whereby, following attenuated

glucose metabolism, p53 engages the intrinsic apoptotic machinery via binding to the anti-apoptotic protein Bcl-xL. Despite minimal cell death, the increased occupancy of Bcl-xL with p53 lowers the apoptotic threshold and creates a dependency on Bcl-xL to block p53-mediated cell death. Targeting this interaction (e.g., BCL-xL inhibition or MDM2 antagonism) liberated p53 from Bcl-xL which coincided with BAX activation and cytoplasmic p53-dependent intrinsic apoptosis. This raises the possibility that "free" cytoplasmic p53 is directly activating BAX to promote apoptosis in response to this therapeutic combination. Finally, it is important to note that while cytoplasmic p53 was necessary for the execution of synergistic apoptosis with either Bcl-xL or MDM2 inhibition, it was universally sufficient only in the context of Bcl-xL inhibition (Supplemental Fig. 7c and Supplemental Fig. 8g). This apparent discrepancy may be explained through observations that, in some instances, the displacement of cytoplasmic p53 from Bcl-xL requires the binding of the p53 transcriptional target gene PUMA[27,43]. As MDM2 antagonists can stimulate nuclear p53 transcriptional activity, including expression of PUMA, it possible that in some contexts the transcription-dependent functions of p53 are required to facilitate cytoplasmic p53-mediated apoptosis in GBM.

It is noteworthy that neither genetic alterations in *EGFR* nor inhibition of EGFR activity were sufficient to predict a metabolic response with EGFR TKI in our GBM samples. Several molecular mechanisms have been described that can enable dynamic compensatory responses to EGFR-directed therapy in GBM[44]. Thus, it is likely that, despite robust inhibition of EGFR, some tumors quickly rewire their molecular circuitry to preserve downstream signaling flux and drive glucose consumption[45]. Given the breadth of potential adaptive mechanisms, coupled with the molecular heterogeneity of GBM, genetic biomarkers may alone be insufficient to predict responses to this approach. Our results emphasize the value of a functional biomarker, in this case changes in glucose uptake[46], as a means to rapidly stratify metabolic responders and non-responders.

Taken together, our findings provide rationale for the clinical evaluation of combined targeting of oncogene-driven glucose metabolism (e.g., EGFRi or PI3Ki) and p53 in GBM patients. Furthermore, we propose a new clinical application of ^{18}F-FDG PET to assess whether targeted drugs have induced a metabolic vulnerability that can be exploited. As we show that changes in ^{18}F-FDG accumulation can be observed within hours of EGFR inhibitor treatment, ^{18}F-FDG PET could serve as a rapid, non-invasive functional biomarker to predict synergistic sensitivity to p53 activation. This non-invasive analysis could be particularly valuable for malignant brain tumors, where pharmacokinetic/pharmacodynamic assessment is extremely difficult and impractical. While there are concerns that ^{18}F-FDG PET cannot properly delineate tumor glucose uptake versus healthy brain tissue glucose uptake, delayed imaging protocols[47] (used here for the mouse studies) and parametric response maps (PRMs) with MRI fusion can be useful for quantifying the changes in tumor ^{18}F-FDG consumption. Lastly, targeting oncogenes that drive glucose uptake in other cancers may evoke similar p53-dependent vulnerabilities. Future work is required to assess the applicability of this concept to other oncogenic drivers and cancers.

Online Methods

Mice

Female NOD *scid* gamma (NSG), 6-8 weeks of age, were purchased from the University of California Los Angeles (UCLA) medical center animal breeding facility. Male CD-1 mice, 6-8 weeks of age, were purchased from Charles River. All mice were kept under defined flora pathogen-free conditions at the AAALAC-approved animal facility of the Division of Laboratory Animals (DLAM) at UCLA. All animal experiments were performed with the approval of the UCLA Office of Animal Resource Oversight (OARO).

Patient-derived GBM cells

All patient tissue to derive GBM cell cultures was obtained through explicit informed consent, using the UCLA Institutional Review Board (IRB) protocol: 10-000655. As previously described[12], primary GBM cells were established and maintained in gliomasphere conditions consisting of DMEM/F12 (Gibco), B27 (Invitrogen), Penicillin-Streptomycin (Invitrogen), and Glutamax (Invitrogen) supplemented with Heparin (5 μg/mL, Sigma), EGF (50 ng/mL, Sigma), and FGF (20 ng/mL, Sigma). All cells were grown at 37°C, 20% O_2, and 5% CO_2 and were routinely monitored and tested negative for the presence of mycoplasma using a commercially available kit (MycoAlert, Lonza). At the time of experiments, most HK lines used were between 20-30 passages (exceptions HK385 p8, HK336 p15), while GS and GBM39 lines were less than 10 passages. All cells were authenticated by short-tandem repeat (STR) analysis.

Reagents and antibodies

Chemical inhibitors from the following sources were dissolved in DMSO for *in vitro* studies: Erlotinib (Chemietek), Nutlin-3A (Selleck Chemicals), WEHI-539 (APExBIO), Pictilisib (Selleck Chemicals), Oligomycin (Sigma), Rotenone (Sigma). 2DG (Sigma) was dissolved freshly in media prior to usage. Antibodies used for immunoblotting were obtained from the listed sources: β-actin (8H10D10) Mouse mAb (Cell signaling, 3700), tubulin (DM1A) Mouse mAb (Cell signaling, 3873), p-EGFR Y1086 (2533287) Rabbit pAb (Thermo Fischer Scientific, 36-9700), t-EGFR Rabbit pAb (Millipore, 06-847), t-AKT (11E7) Rabbit mAb (Cell Signaling, 4685), p-AKT T308 (D25E6) Rabbit mAb (Cell Signaling, 13038), p-AKT S473 (D9E) Rabbit mAb (Cell Signaling, 4060), t-ERK (137F5) Rabbit mAb (Cell Signaling, 4695), p-ERK T202/Y204 (D13.14.4E) Rabbit mAb (Cell Signaling, 4370), t-S6 (5G10) Rabbit mAb (Cell Signaling, 2217), p-S6 S235/236 (D57.2.2E) Rabbit mAb (Cell Signaling, 4858), t-4EBP1 (53H11) Rabbit mAb (Cell Signaling, 9644), p-4EBP1 S65 Rabbit pAb (Cell Signaling 9451), Glut3 Rabbit pAb (Abcam, ab15311), Glut1 Rabbit pAb (Millipore, 07-1401), p53 (DO-1) Mouse mAb (Santa Cruz Biotechnology, SC-126), BAX (D2E11) Rabbit mAb (Cell Signaling, 5023), BIM (C34C5) Rabbit mAb (Cell Signaling, 2933), PUMA (D30C10) Rabbit mAb (Cell Signaling, 12450), Bcl-2 (50E3) Rabbit mAb (Cell Signaling, 2870), Bcl-xL (54H6) Rabbit mAb (Cell Signaling, 2764), Mcl-1 (D35A5) Rabbit mAb (Cell Signaling, 5453), Cytochrome c Rabbit pAb (Cell Signaling, 4272), and Cleaved Caspase-3 Rabbit pAb (Cell Signaling, 9661). Antibodies used for immunoprecipitation were obtained from the listed sources: p53 Rabbit pAb (Cell Signaling, 9282). Secondary antibodies were obtained from

the listed sources: Anti-rabbit IgG HRP-linked (Cell Signaling, 7074) and Anti-mouse IgG HRP-linked (Cell Signaling, 7076). All immunoblotting antibodies were used at a dilution of 1:1000, except β-actin and tubulin, which were used at 1:10,000. Immunoprecipitation antibodies were diluted according to manufacturer's instructions (1:200 for p53). Secondary antibodies were used at a dilution of 1:5000.

^{18}F-Fluorodeoxyglucose (^{18}F-FDG) uptake assay

Cells were plated at 5×10^4 cells/ml and treated with designated drugs for indicated time points. Following appropriate treatment, cells were collected and resuspended in glucose-free DMEM/F12 (US Biological) containing ^{18}F-FDG (radioactivity 1 μCi/mL). Cells were incubated at 37°C for 1 hr and then washed three times with ice cold PBS. Radioactivity of each sample was then measured using a gamma counter.

Glucose, glutamine, and lactate measurements

Cellular glucose consumption and lactate production were measured using a Nova Biomedical BioProfile Basic Analyzer. Briefly, cells were plated in 1×10^5 cells/ml in 2 mL of gliomasphere conditions and appropriate drug conditions. 12 hrs following drug treatment, 1 ml of media was removed from each sample and analyzed in the Nova BioProfile analyzer. Measurements were normalized to cell number.

Annexin V apoptosis assay

Cells were collected and analyzed for Annexin V and PI staining according to manufacturer's protocol (BD Biosciences). Briefly, cells were plated at 5×10^4 cells/ml and treated with appropriate drugs. Following indicated time points, cells were collected, trypsinized, washed with PBS, and stained with Annexin V and PI for 15 minutes. Samples were then analyzed using the BD LSRII flow cytometer.

Immunoblotting

Cells were collected and lysed in RIPA buffer (Boston BioProducts) containing Halt Protease and Phosphatase Inhibitor (Thermo Fischer Scientific). Lysates were centrifuged at 14,000×g for 15min at 4°C. Protein samples were then boiled in NuPAGE LDS Sample Buffer (Invitrogen) and NuPAGE Sample Reducing Agent (Invitrogen) and separated using SDS-PAGE on 12% Bis-Tris gels (Invitrogen) and transferred to nitrocellulose membrane (GE Healthcare). Immunoblotting was performed per antibody's manufacturer's specifications and as mentioned previously. Membranes were developed using the SuperSignal system (Thermo Fischer Scientific).

Immunoprecipitation

Cells were collected, washed once with PBS, and incubated in IP lysis buffer (25 mM Tris-HCL pH 7.4, 150 mM NaCl, 1 mM EDTA, 1% NP-40, 5% Glycerol) at 4°C for 15 minutes. 300-500 μg of each sample was then pre-cleared in Protein A/G Plus Agarose Beads (Thermo Fischer Scientific) for one hour. Following pre-clear, samples were then incubated with antibody-bead conjugates overnight according to manufacturer's specifications and as mentioned previously. The samples were then centrifuged at 1000g for 1 min, and the beads

were washed with 500 μL of IP lysis buffer for five times. Proteins were eluted from the beads by boiling in 2× LDS Sample Buffer (Invitrogen) at 95°C for 5 min. Samples analyzed by immunoblotting as previously described. Immunoprecipitation antibodies were diluted according to manufacturer's instructions (1:200 for p53 and 1:100 for Bcl-xL).

Dynamic BH3 profiling

GBM gliomaspheres were first disassociated to single-cell suspensions with TrypLE (Gibco) and resuspended in MEB buffer (150 mM Mannitol 10 mM HEPES-KOH, 50 mM KCl, 0.02 mM EGTA, 0.02 mM EDTA, 0.1 % BSA, 5 mM Succinate). 50μl of cell suspension (3×10^4 cells/well) were plated in wells holding 50 μL MEB buffer containing 0.002% digitonin and indicated peptides in 96-well plates. Plates were then incubated at 25°C for 50 min. Cells were then fixed with 4% paraformaldehyde for 10min, followed by neutralization with N2 buffer (1.7M Tris, 1.25M Glycine pH 9.1) for 5min. Samples were stained overnight with 20 μL of staining solution (10% BSA, 2% Tween 20 in PBS) containing DAPI and anti-cytochrome c (BioLegend). The following day, cytochrome c release was quantified using BD LSRII flow cytometer. Measurements were normalized to appropriate controls that do not promote cytochrome c release (DMSO and inactive PUMA2A peptide). Delta priming refers to the difference in amount of cytochrome c release between vehicle treated cells and drug treated cells.

Plasma membrane protein extraction

1×10^7 cells were treated with indicated drugs. Following 4hr of treatment, cells were collected, washed once with ice cold PBS, and lysed using a Dounce Homogenizer. Plasma membrane protein extraction proceeded following manufacturer's protocol (BioVision), and isolated proteins were then subject to immunoblotting.

BAX oligomerization

7.5×10^5 cells were treated with indicated drugs. Following 24 hr of treatment, cells were collected, washed once with ice cold PBS, and re-suspended in 1 mM bismaleimidohexane (BMH) in PBS for 30 min. Cells were then pelleted and lysed for immunoblotting, as described above.

Cytochrome *c* detection

5 million cells were plated at a concentration of 1×10^5 cells/mL and treated with indicated drugs. Following 24 hr of treatment, cells were collected, washed once with ice cold PBS. Subcellular fractionation was then performed using a mitochondrial isolation kit (Thermo Fischer Scientific, 89874). Both cytoplasmic and mitochondrial fractions were subjected to immunoblotting and cytochrome c was detected using cytochrome c antibody at a dilution of 1:1000 (Cell Signaling, 4272).

Mouse xenograft studies

For intracranial experiments, GBM39, HK336, HK393, and GS025 cells were injected (4×10^5 cells per injection) into the right striatum of the brain of female NSG mice (6-8 weeks old). Injection coordinates were 2 mm lateral and 1 mm posterior to bregma, at a depth of 2

mm. Tumor burden was monitored by secreted *gaussia* luciferase and following three consecutive growth measurements, mice were randomized into four treatment arms consisting of appropriate vehicles, 75 mg/kg erlotinib, 50 mg/kg Idasanutlin, or a combination of both drugs. Vehicle consisted of 0.5% methylcellulose in water, which is used to dissolve erlotinib, and a proprietary formulation obtained from Roche, which is used to dissolve Idasanutlin. Tumor burden was assessed twice per week by secreted *gaussia* luciferase. When possible, mice were treated for 25 days and taken off treatment and monitored for survival. Drugs were administered through oral gavage. Sample sizes were chosen based off estimates from pilot experiments and results from previous literature[12]. Investigators were not blinded to group allocation or assessment of outcome. All studies were in accordance with UCLA OARO protocol guidelines.

Intracranial delayed PET/CT mouse imaging

For baseline ^{18}F-FDG scans, mice were treated with vehicle and 15 hours later were pre-warmed, anesthetized with 2% isoflurane, and intravenously injected with 70 μCi of ^{18}F-FDG. Following 1hr unconscious uptake, mice were taken off anesthesia but kept warm for another 5 hr of uptake. 6 hr after the initial administration of ^{18}F-FDG, mice were imaged using G8 PET/CT scanner (Sofie Biosciences). Following imaging, all mice were then dosed with erlotinib (75 mg/kg) and 15 hours later went through the same imaging procedure. Per above, quantification was performed by drawing 3D regions of interest (ROI) using the AMIDE software as previously described[48]. Note, the 15 hour treatment time point was the earliest time point that fit within the logistical constraints; this includes half-lives required for adequate probe decay for subsequent imaging, ^{18}F-FDG production schedule and imaging center hours.

Immunohistochemistry

Immunohistochemistry was performed on 4 μm sections that were cut from FFPE (formalin-fixed, paraffin-embedded) blocks. Sections were then deparaffinised with xylene and rehydrated through graded ethanol. Antigen retrieval was achieved with a pH 9.5 Nuclear Decloaker (Biocare Medical) in a Decloaking pressure cooker at 95°C for 40 min. Tissue sections were then treated with 3% hydrogen peroxide (LOT 161509; Fisher Chemical) and with Background Sniper (Biocare Medical, Concord, CA, USA) to reduce nonspecific background staining. Primary antibody for p53 (Cell Signaling, 2527) was applied in a 1:150 dilution for 80 min followed by detection with the MACH 3 Rabbit HRP- Polymer Detection kit (Biocare Medical). Visualization was achieved using VECTOR NovaRED (SK-4800; Vector Laboratories, Inc.) as chromogen. Lastly, sections were counterstained with Tacha's Automated Hematoxylin (Biocare Medical).

Quantitative RT-PCR

RNA was extracted from all cells using Purelink RNA Kit (Invitrogen). cDNA was synthesized with iScript cDNA Synthesis Kit (Bio-Rad) as per manufacturer's instructions. Quantitative PCR (qPCR) was conducted on the Roche LightCycler 480 using SYBRGreen Master Mix (Kapa Biosciences). Relative expression values are normalized to control gene (*GAPDH*). Primer sequences are as listed (5′ to 3′): *P21* (forward GACTTTGTCACCGAGACACC, reverse GACAGGTCCACATGGTCTTC), *PUMA*

(forward ACGACCTCAACGCACAGTACG, reverse GTAAGGGCAGGAGTCCCATGATG), *GAPDH* (forward TGCCATGTAGACCCCTTGAAG, reverse ATGGTACATGACAAGGTGCGG), *MDM2* (forward CTGTGTTCAGTGGCGATTGG, reverse AGGGTCTCTTGTTCCGAAGC), *TIGAR* (forward GGAAGAGTGCCCTGTGTTTAC, reverse GACTCAAGACTTCGGGAAAGG), *PIG3* (forward GCAGCTGCTGGATTCAATTA, reverse TCCCAGTAGGATCCGCCTAT)

P53 reporter activity

Cells were first infected with lentivirus synthesized from a p53 reporter plasmid which codes for luciferase under the control of a p53 responsive element: TACAGAACATGTCTAAGCATGCTGTGCCTTGCCTGGACTTGCCTGGCCTTGCCTTGGG. Infected cells were then plated into a 96-well plate at 5,000 cells/ 50 μL and treated with indicated drugs for 24 hr and then incubated with 1 mM D-luciferin for two hours. Bioluminescence was measured using IVIS Lumina II (Perkin Elmer).

Genetic manipulation

In general, lentivirus used for genetic manipulation were produced by transfecting 293-FT cells (Thermo) using Lipofectamine 2000 (Invitrogen). Virus was collected 48 hours after transfection. The lentiviral sgp53 vector and sgControl vector contained the following guide RNA, respectively: CCGGTTCATGCCGCCCATGC and GTAATCCTAGCACTTTTAGG. LentiCRISPR-v2 was used as the backbone. Glut1 and Glut3 cDNA was cloned from commercially available vectors and incorporated into pLenti-GLuc-IRES-EGFP lentiviral backbone containing a CMV promoter (Glut1 was a gift from Wolf Frommer (Addgene #18085[49]), Glut3 was obtained from OriGene #SC115791, and the lentiviral backbone was obtained from Targeting Systems #GL-GFP). pMIG Bcl-xL was a gift from Stanley Korsmeyer (Addgene #8790[50]) and cloned into the lentiviral backbone mentioned above (Targeting Systems). Cytoplasmic (K305A and R306A) and wild-type p53 constructs were a kind gift from R. Agami and G. Lahav. The genes of interest were cloned into a lentiviral vector containing a PGK promoter. Constructs for p53 DNA binding domain mutants (R175H) and (R273H) as well as the nuclear mutant (L348A and L350A) were generated using site-directed mutagenesis (New England Biolabs #E0554S) on the wild-type p53 construct.

For EGFR knockdown experiments, siRNA against EGFR (Thermo Fischer Scientific, s563) was transfected into cells using DharmaFECT 4 (Dharmacon). Following 48 hours, cells were harvested and used for indicated experiments.

Immunofluorescence

For immunofluorescence, gliomaspheres were first disassociated to single cell and adhered to the 96-well plates using Cell-Tak (Corning) according to manufacturer instructions. Adhered cells were then fixed with ice-cold methanol for 10 min then washed three times with PBS. Cells were then incubated with blocking solution containing 10% FBS and 3% BSA in PBS for 1 hr and subsequently incubated with p53 (Santa Cruz, SC-126, dilution of 1:50) antibody overnight at 4°C. The following day, cells were incubated with secondary

antibody (Alexa Fluor 647, dilution 1:2000) for an hour and DAPI staining for 10 min, then imaged using a Nikon TI Eclipse microscope equipped with a Cascade II fluorescent camera (Roper Scientific). Cells were imaged with emissions at 461 nM and 647 nM and then processed using NIS-Elements AR analysis software.

Oxygen consumption rate (OCR) and extracellular acidification rate (ECAR) measurements

For metabolic measurements involving OCR and ECAR, gliomaspheres treated with indicated drugs were first disassociated to single-cell suspensions and adhered to XF24 plates (Seahorse Bioscience) using Cell-Tak (Corning) according to manufacturer instructions. Prior to the assay, cells were supplemented with unbuffered DMEM, and incubated at 37°C for 30 min before starting OCR and ECAR measurements. Basal ECAR measurements between control and erlotinib treated cells are shown.

Mass-spectroscopy sample preparation

Male CD-1 mice (6-8 weeks old) were treated with 50 mg/kg Idasanutlin in duplicate through oral gavage. At 0.5, 1, 2, 4, 6, 8, 12, and 24 hr after administration, mice were sacrificed, blood was harvested by retro-orbital bleeding, and brain tissue was collected. Whole blood from mice was centrifuged to isolate plasma. Idasanutlin was isolated by liquid-liquid extraction from plasma: 50 μL plasma was added to 2 μL internal standard and 100 μL acetonitrile. Mouse brain tissue was washed with 2 mL cold PBS and homogenized using a tissue homogenizer with fresh 2 mL cold PBS. Idasanutlin was then isolated and reconstituted in a similar manner by liquid-liquid extraction: 100 μL brain homogenate was added to 2 μL internal standard and 200 μL acetonitrile. After vortex mixing, the samples was centrifuged. The supernatant was removed and evaporated by a rotary evaporator and reconstituted in 100 μL 50:50 water: acetonitrile.

Idasanutlin detection by mass-spectrometry

Chromatographic separations were performed on a 100×2.1 mm Phenomenex Kinetex C18 column (Kinetex) using the 1290 Infinity LC system (Agilent). The mobile phase was composed of solvent A: 0.1% formic acid in Milli-Q water, and B: 0.1% formic acid in acetonitrile. Analytes were eluted with a gradient of 5% B (0-4 min), 5-99% B (4-32 min), 99% B (32-36 min), and then returned to 5% B for 12 min to re-equilibrate between injections. Injections of 20 μL into the chromatographic system were used with a solvent flow rate of 0.10 mL/min. Mass spectrometry was performed on the 6460 triple quadrupole LC/MS system (Agilent). Ionization was achieved by using electrospray in the positive mode and data acquisition was made in multiple reactions monitoring (MRM) mode. The MRM transition used for Idasanutlin detection was m/z 616.2 → 421.2 with fragmentor voltage of 114V, and collision energy of 20 eV. Analyte signal was normalized to the internal standard and concentrations were determined by comparison to the calibration curve (0.5, 5, 50, 250, 500, 2000 nM). Idasanutlin brain concentrations were adjusted by 1.4% of the mouse brain weight for the residual blood in the brain vasculature as described by Dai et al [51].

Secreted *gaussia* luciferase measurements

Cells were infected with a lentiviral vector containing secreted *gaussia* luciferase (sGluc) reporter gene (Targeting Systems # GL-GFP) and intracranially implanted into the right striatum of mice (4×10^5 cells/mouse). To measure the levels of secreted Gaussia luciferase (sGluc), 6 μL of blood was collected from the tail vein of the mice and immediately mixed with 50 mM EDTA to prevent coagulation. Gluc activity was obtained by measuring chemiluminescence following injection of 100 μL of 100 μM coelentarazine (Nanolight) in a 96 well plate as described before.[38]

Synergy score calculations

1.0×10^5 GBM cells were plated in triplicate and treated with erlotinib, nutlin, or combination at multiple concentrations using a matrix where each drug was added to the cells at six concentrations (0-10 μM). Annexin V staining was measured following 72 hrs of treatment. Using the Chalice software, as described in Lehar et al., the response of the combination was compared to its single agents, and the combinatorial effects were calculated using the synergy score[33].

DNA sequencing

Targeted sequencing was performed for samples HK206, HK217, HK250, HK296 for the following genes *BCL11A, BCL11B, BRAF, CDKN2A, CHEK2, EGFR, ERBB2, IDH1, IDH2, MSH6, NF1, PIK3CA, PIK3R1, PTEN, RB1, TP53* using Illumina Miseq. There were 1 to 2 million reads per sample with average coverage of 230 per gene. Copy number variants were determined for these samples using a whole genome SNP array. The genetic profile of GBM39 has been previously reported[45].

Whole exome sequencing was performed for samples HK157, HK229, HK248, HK250, HK254, HK296, HK301, HK336, HK350, HK390, HK393 and carried out at SeqWright. Samples were grouped into 2 pools with separate capture reactions. Nextera Rapid capture and library preparation were used and sequencing performed on a HiSeq 2500, 2×100 bp with 100× on-target coverage, 2 full rapid runs, each with 1 normal diploid control. Copy number analysis for these samples was carried out using EXCAVATOR software: http://genomebiology.com/content/pdf/gb-2013-14-10-r120.pdf

Data-availability statement

Data presented in this manuscript are available from the corresponding authors upon request.

Annotation of TCGA samples

273 GBM samples from the TCGA were analyzed for genetic alterations in EGFR, p53 and p53-regulated pathways. Co-occurrences of mutations were examined and only significant interactions are displayed. Data was analyzed using cBioPortal as previously described [52,53].

Fluorescence *in situ* Hybridization (FISH)

Fluorescence in situ hybridization (FISH) was performed using commercially available fluorescently labeled dual-color EGFR (red)/CEP 7(green) probe (Abbott-Molecular). FISH

hybridization and analyses were performed on cell lines, following the manufacturer's suggested protocols. The cells were counterstained with DAPI and the fluorescent probe signals were imaged under a Zeiss (Axiophot) Fluorescent Microscope equipped with dual- and triple-color filters.

Statistical analysis

Comparisons were made using two-tailed unpaired Student's *t*-tests and *p* values <0.05 were considered statistically significant. All data from multiple independent experiments were assumed to be of normal variance. For each experiment, replicates are as noted in the figure legends. Data represent mean ± s.d. values unless otherwise indicated. All statistical analyses were calculated using Prism 7.0 (GraphPad). For all *in vitro* and *in vivo* experiments, no statistical method was used to predetermine sample size and no samples were excluded. For *in vivo* tumor measurements, the last data sets were used for comparisons between groups. As described above, all mice were randomized before studies.

Supplementary Material

Refer to Web version on PubMed Central for supplementary material.

Acknowledgments

References

1. Brennan CW, et al. The somatic genomic landscape of glioblastoma. Cell. 2013; 155:462–477. DOI: 10.1016/j.cell.2013.09.034 [PubMed: 24120142]

2. Vivanco I, et al. Differential sensitivity of glioma- versus lung cancer-specific EGFR mutations to EGFR kinase inhibitors. Cancer Discov. 2012; 2:458–471. doi:2159-8290.CD-11-0284 [pii]. 10.1158/2159-8290.CD-11-0284. [PubMed: 22588883]

3. Cloughesy TF, Cavenee WK, Mischel PS. Glioblastoma: from molecular pathology to targeted treatment. Annu Rev Pathol. 2014; 9:1–25. DOI: 10.1146/annurev-pathol-011110-130324 [PubMed: 23937436]

4. Lee EQ, et al. Phase I/II study of sorafenib in combination with temsirolimus for recurrent glioblastoma or gliosarcoma: North American Brain Tumor Consortium study 05-02. Neuro Oncol. 2012; 14:1511–1518. DOI: 10.1093/neuonc/nos264 [PubMed: 23099651]

5. Wen PY, et al. Phase I/II study of erlotinib and temsirolimus for patients with recurrent malignant gliomas: North American Brain Tumor Consortium trial 04-02. Neuro Oncol. 2014; 16:567–578. DOI: 10.1093/neuonc/not247 [PubMed: 24470557]

6. Lee, Michael J., et al. Sequential Application of Anticancer Drugs Enhances Cell Death by Rewiring Apoptotic Signaling Networks. Cell. 2012; 149:780–794. doi: http://dx.doi.org/10.1016/j.cell.2012.03.031. [PubMed: 22579283]

7. Vander Heiden MG, et al. Growth factors can influence cell growth and survival through effects on glucose metabolism. Molecular and cellular biology. 2001; 21:5899–5912. [PubMed: 11486029]

8. Altman BJ, Rathmell JC. Metabolic stress in autophagy and cell death pathways. Cold Spring Harb Perspect Biol. 2012; 4:a008763. [PubMed: 22952396]

9. Verhaak RGW, et al. An integrated genomic analysis identifies clinically relevant subtypes of glioblastoma characterized by abnormalities in PDGFRA, IDH1, EGFR and NF1. Cancer cell. 2010; 17:98. [PubMed: 20129251]

10. Babic I, et al. EGFR mutation-induced alternative splicing of Max contributes to growth of glycolytic tumors in brain cancer. Cell Metab. 2013; 17:1000–1008. DOI: 10.1016/j.cmet.2013.04.013 [PubMed: 23707073]

11. Lee J, et al. Tumor stem cells derived from glioblastomas cultured in bFGF and EGF more closely mirror the phenotype and genotype of primary tumors than do serum-cultured cell lines. Cancer Cell. 2006; 9:391–403. doi:S1535-6108(06)00117-6 [pii]. 10.1016/j.ccr.2006.03.030. [PubMed: 16697959]

12. Nathanson DA, et al. Targeted therapy resistance mediated by dynamic regulation of extrachromosomal mutant EGFR DNA. Science. 2014; 343:72–76. DOI: 10.1126/science.1241328 [PubMed: 24310612]

13. Masui K, et al. mTOR complex 2 controls glycolytic metabolism in glioblastoma through FoxO acetylation and upregulation of c-Myc. Cell Metab. 2013; 18:726–739. DOI: 10.1016/j.cmet.2013.09.013 [PubMed: 24140020]

14. Haq R, et al. Oncogenic BRAF regulates oxidative metabolism via PGC1alpha and MITF. Cancer Cell. 2013; 23:302–315. DOI: 10.1016/j.ccr.2013.02.003 [PubMed: 23477830]

15. Zhao Y, et al. Glucose metabolism attenuates p53 and Puma-dependent cell death upon growth factor deprivation. J Biol Chem. 2008; 283:36344–36353. DOI: 10.1074/jbc.M803580200 [PubMed: 18990690]

16. Deng J, et al. BH3 profiling identifies three distinct classes of apoptotic blocks to predict response to ABT-737 and conventional chemotherapeutic agents. Cancer Cell. 2007; 12:171–185. DOI: 10.1016/j.ccr.2007.07.001 [PubMed: 17692808]

17. Montero J, et al. Drug-induced death signaling strategy rapidly predicts cancer response to chemotherapy. Cell. 2015; 160:977–989. DOI: 10.1016/j.cell.2015.01.042 [PubMed: 25723171]

18. Kruse JP, Gu W. Modes of p53 regulation. Cell. 2009; 137:609–622. DOI: 10.1016/j.cell.2009.04.050 [PubMed: 19450511]

19. Maddocks OD, Vousden KH. Metabolic regulation by p53. J Mol Med (Berl). 2011; 89:237–245. DOI: 10.1007/s00109-011-0735-5 [PubMed: 21340684]

20. Jiang D, et al. Analysis of p53 transactivation domain mutants reveals Acad11 as a metabolic target important for p53 pro-survival function. Cell reports. 2015; 10:1096–1109. DOI: 10.1016/j.celrep.2015.01.043 [PubMed: 25704813]

21. Chipuk JE, et al. Direct activation of Bax by p53 mediates mitochondrial membrane permeabilization and apoptosis. Science. 2004; 303:1010–1014. DOI: 10.1126/science.1092734 [PubMed: 14963330]

22. Mihara M, et al. p53 Has a Direct Apoptogenic Role at the Mitochondria. Molecular Cell. 2003; 11:577–590. doi: http://dx.doi.org/10.1016/S1097-2765(03)00050-9. [PubMed: 12667443]

23. Liu JC, et al. High mitochondrial priming sensitizes hESCs to DNA-damage-induced apoptosis. Cell Stem Cell. 2013; 13:483–491. DOI: 10.1016/j.stem.2013.07.018 [PubMed: 23954752]

24. Strom E, et al. Small-molecule inhibitor of p53 binding to mitochondria protects mice from gamma radiation. Nat Chem Biol. 2006; 2:474–479. doi: http://www.nature.com/nchembio/journal/v2/n9/suppinfo/nchembio809_S1.html. [PubMed: 16862141]

25. Tasdemir E, et al. Regulation of autophagy by cytoplasmic p53. Nature cell biology. 2008; 10:676–687. DOI: 10.1038/ncb1730 [PubMed: 18454141]

26. Green DR, Kroemer G. Cytoplasmic functions of the tumour suppressor p53. Nature. 2009; 458:1127–1130. DOI: 10.1038/nature07986 [PubMed: 19407794]

27. Chipuk JE, Bouchier-Hayes L, Kuwana T, Newmeyer DD, Green DR. PUMA couples the nuclear and cytoplasmic proapoptotic function of p53. Science. 2005; 309:1732–1735. DOI: 10.1126/science.1114297 [PubMed: 16151013]

28. Lessene G, et al. Structure-guided design of a selective BCL-XL inhibitor. Nat Chem Biol. 2013; 9:390–397. http://www.nature.com/nchembio/journal/v9/n6/abs/nchembio.1246.html#supplementary-information. DOI: 10.1038/nchembio.1246 [PubMed: 23603658]

29. Comprehensive genomic characterization defines human glioblastoma genes and core pathways. Nature. 2008; 455:1061–1068. doi:nature07385 [pii]. 10.1038/nature07385. [PubMed: 18772890]

30. Zhang Y, Xiong Y, Yarbrough WG. ARF Promotes MDM2 Degradation and Stabilizes p53: ARF-INK4a Locus Deletion Impairs Both the Rb and p53 Tumor Suppression Pathways. Cell. 1998; 92:725–734. doi: http://dx.doi.org/10.1016/S0092-8674(00)81401-4. [PubMed: 9529249]

31. Pomerantz J, et al. The Ink4a tumor suppressor gene product, p19Arf, interacts with MDM2 and neutralizes MDM2's inhibition of p53. Cell. 1998; 92:713–723. [PubMed: 9529248]

32. Tovar C, et al. Small-molecule MDM2 antagonists reveal aberrant p53 signaling in cancer: implications for therapy. Proc Natl Acad Sci U S A. 2006; 103:1888–1893. DOI: 10.1073/pnas.0507493103 [PubMed: 16443686]

33. Lehar J, et al. Synergistic drug combinations tend to improve therapeutically relevant selectivity. Nat Biotechnol. 2009; 27:659–666. DOI: 10.1038/nbt.1549 [PubMed: 19581876]

34. Vaseva AV, Marchenko ND, Moll U. The transcription-independent mitochondrial p53 program is a major contributor to Nutlin-induced apoptosis in tumor cells. Cell Cycle. 2009; 8:1711–1719. DOI: 10.4161/cc.8.11.8596 [PubMed: 19411846]

35. Chipuk JE, Maurer U, Green DR, Schuler M. Pharmacologic activation of p53 elicits Bax-dependent apoptosis in the absence of transcription. Cancer cell. 2003; 4:371–381. doi: http://dx.doi.org/10.1016/S1535-6108(03)00272-1. [PubMed: 14667504]

36. DeBerardinis RJ, Lum JJ, Hatzivassiliou G, Thompson CB. The biology of cancer: metabolic reprogramming fuels cell growth and proliferation. Cell Metab. 2008; 7:11–20. doi:S1550-4131(07)00295-1 [pii]. 10.1016/j.cmet.2007.10.002. [PubMed: 18177721]

37. Ding Q, et al. Discovery of RG7388, a potent and selective p53-MDM2 inhibitor in clinical development. J Med Chem. 2013; 56:5979–5983. DOI: 10.1021/jm400487c [PubMed: 23808545]

38. Tannous BA. Gaussia luciferase reporter assay for monitoring biological processes in culture and in vivo. Nat Protoc. 2009; 4:582–591. doi:nprot.2009.28 [pii]. 10.1038/nprot.2009.28. [PubMed: 19373229]

39. Qu L, et al. Endoplasmic reticulum stress induces p53 cytoplasmic localization and prevents p53-dependent apoptosis by a pathway involving glycogen synthase kinase-3β. Genes & Development. 2004; 18:261–277. DOI: 10.1101/gad.1165804 [PubMed: 14744935]

40. Han MK, et al. SIRT1 Regulates Apoptosis and Nanog Expression in Mouse Embryonic Stem Cells by Controlling p53 Subcellular Localization. Cell Stem Cell. 2:241–251. DOI: 10.1016/j.stem.2008.01.002

41. Yang WH, et al. Modification of p53 with O-linked N-acetylglucosamine regulates p53 activity and stability. Nature cell biology. 2006; 8:1074–1083. doi: http://www.nature.com/ncb/journal/v8/n10/suppinfo/ncb1470_S1.html. [PubMed: 16964247]

42. Leu JIJ, Dumont P, Hafey M, Murphy ME, George DL. Mitochondrial p53 activates Bak and causes disruption of a Bak-Mcl1 complex. Nat Cell Biol. 2004; 6:443–450. [PubMed: 15077116]

43. Follis AV, et al. PUMA binding induces partial unfolding within BCL-xL to disrupt p53 binding and promote apoptosis. Nat Chem Biol. 2013; 9:163–168. doi:http://www.nature.com/nchembio/journal/v9/n3/abs/nchembio.1166.html#supplementary-information. [PubMed: 23340338]

44. Reardon DA, Wen PY, Mellinghoff IK. Targeted molecular therapies against epidermal growth factor receptor: past experiences and challenges. Neuro Oncol. 2014; 16(Suppl 8):viii7–13. DOI: 10.1093/neuonc/nou232 [PubMed: 25342602]

45. Wei W, et al. Single-Cell Phosphoproteomics Resolves Adaptive Signaling Dynamics and Informs Targeted Combination Therapy in Glioblastoma. Cancer Cell. 2016; 29:563–573. DOI: 10.1016/j.ccell.2016.03.012 [PubMed: 27070703]

46. Clark PM, Ebiana VA, Gosa L, Cloughesy TF, Nathanson DA. Harnessing Preclinical Molecular Imaging to Inform Advances in Personalized Cancer Medicine. Journal of Nuclear Medicine. 2017; 58:689–696. DOI: 10.2967/jnumed.116.181693 [PubMed: 28385796]

47. Spence AM, et al. 18F-FDG PET of Gliomas at Delayed Intervals: Improved Distinction Between Tumor and Normal Gray Matter. Journal of Nuclear Medicine. 2004; 45:1653–1659. [PubMed: 15471829]

48. Nathanson DA, et al. Co-targeting of convergent nucleotide biosynthetic pathways for leukemia eradication. The Journal of experimental medicine. 2014; 211:473–486. DOI: 10.1084/jem. 20131738 [PubMed: 24567448]

49. Takanaga H, Frommer WB. Facilitative plasma membrane transporters function during ER transit. FASEB J. 2010; 24:2849–2858. DOI: 10.1096/fj.09-146472 [PubMed: 20354141]

50. Cheng EH, et al. BCL-2, BCL-X(L) sequester BH3 domain-only molecules preventing BAX- and BAK-mediated mitochondrial apoptosis. Molecular cell. 2001; 8:705–711. [PubMed: 11583631]

51. Dai H, Marbach P, Lemaire M, Hayes M, Elmquist WF. Distribution of STI-571 to the Brain Is Limited by P-Glycoprotein-Mediated Efflux. Journal of Pharmacology and Experimental Therapeutics. 2003; 304:1085–1092. DOI: 10.1124/jpet.102.045260 [PubMed: 12604685]

52. Gao J, et al. Integrative analysis of complex cancer genomics and clinical profiles using the cBioPortal. Sci Signal. 2013; 6:pl1. [PubMed: 23550210]

53. Cerami E, et al. The cBio cancer genomics portal: an open platform for exploring multidimensional cancer genomics data. Cancer discovery. 2012; 2:401–404. DOI: 10.1158/2159-8290.CD-12-0095 [PubMed: 22588877]
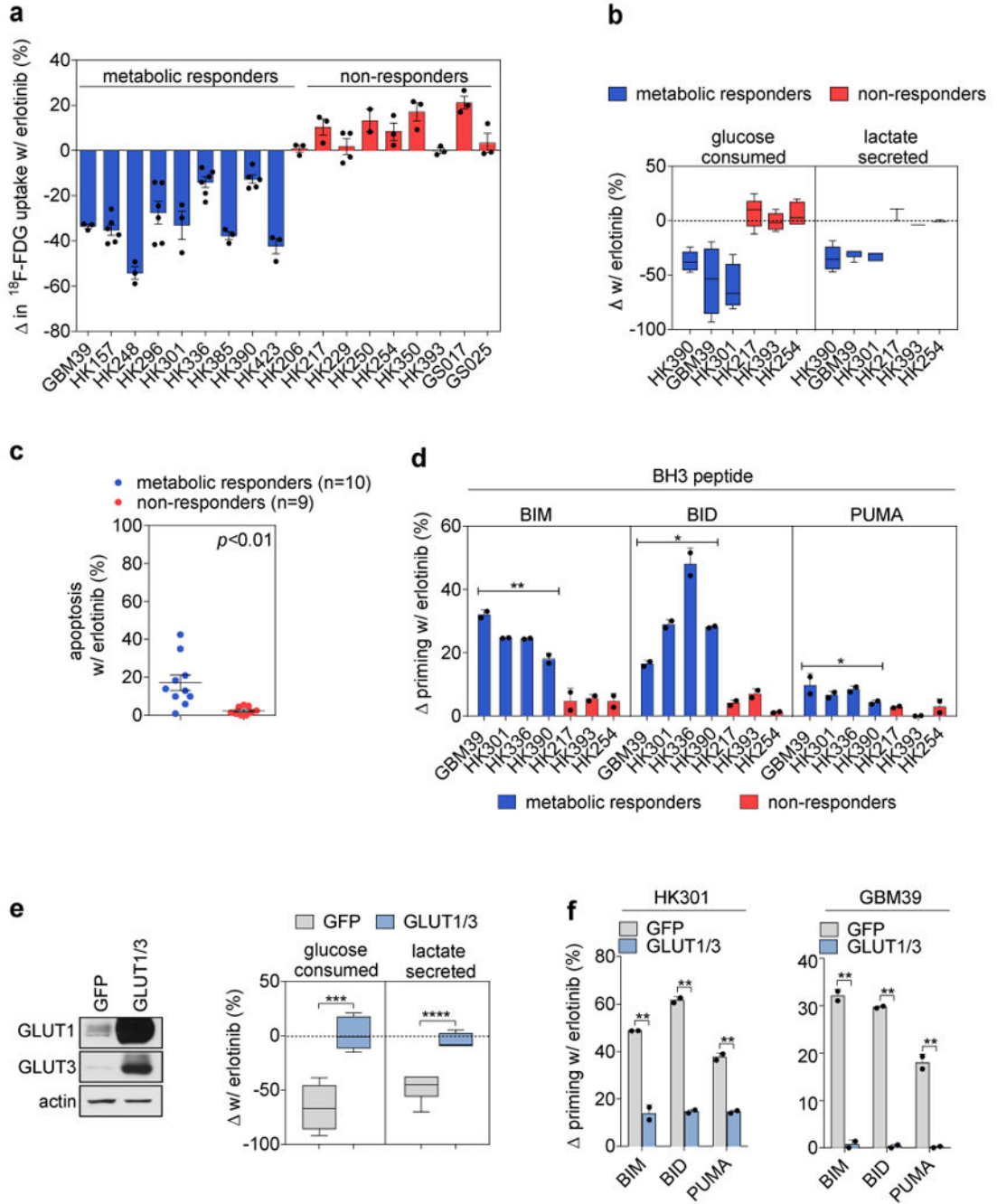
Figure 1. Inhibition of EGFR-driven glucose metabolism induces minimal cell death but primes GBM cells for apoptosis

(a) Percent change in ^{18}F-FDG uptake after 4 hours of 1 μM erlotinib treatment relative to vehicle in 19 patient-derived GBM gliomaspheres. Concentration of erlotinib was selected to achieve robust inhibition of EGFR activity across our panel of primary GBM cells (see Supplemental Fig. 2). "Metabolic responders" (blue) are samples that show a significant decrease in ^{18}F-FDG uptake relative to vehicle, whereas "non-responders" (red) show no significant decrease (mean ± s.d., n 3). (b) % change in glucose consumption and lactate

secretion with 12 hours of 1 μM erlotinib treatment relative to vehicle. Measurements were made using Nova Biomedical BioProfile Analyzer (mean ± s.d., n 5). **(c)** Annexin V staining of metabolic responders (blue, $n = 10$ unique gliomaspheres) or non-responders (red, $n = 9$ unique gliomaspheres) after treatment with 1 μM erlotinib for 72 hours. Each point represents the mean apoptosis of two independent experiments conducted for each gliomasphere sample. See Supplementary Fig. 11 for flow cytometry gating strategy. **(d)** The % change, relative to vehicle control, in priming as determined by cytochrome c release following exposure to each BH3 peptide (BIM, BID, or PUMA) in metabolic responders or non-responders treated with 1 μM erlotinib for 24 hours (mean ± s.d., $n = 2$). Statistical analysis was performed on the grouped metabolic responders versus non-responders. Results are representative of two independent experiments **(e)** Left: Immunoblot of whole cell lysate of HK301 cells overexpressing GFP control or GLUT1 and GLUT3 (GLUT1/3). Right: Changes in glucose consumption or lactate secretion of HK301-GFP or HK301-GLUT1/3 after 12 hours of 1 μM erlotinib treatment. Values are relative to vehicle control (mean ± s.d., n 5). **(f)** Same as (d) using HK301-GFP or HK301-GLUT1/3 cells (left) or GBM39-GFP or GBM39-GLUT1/3 cells (right). In the box plots, the central rectangle spans the first quartile to the third quartile (the interquartile range or IQR), the central line inside the rectangle shows the mean, and whiskers above and below the box show the locations of the minimum and maximum within 1.5 IQR of the lower quartile and the upper quartile, respectively. Comparisons were made using two-tailed unpaired Student's t-test. *p<0.05, **p<0.01, ***p<0.001, ****p<0.0001.
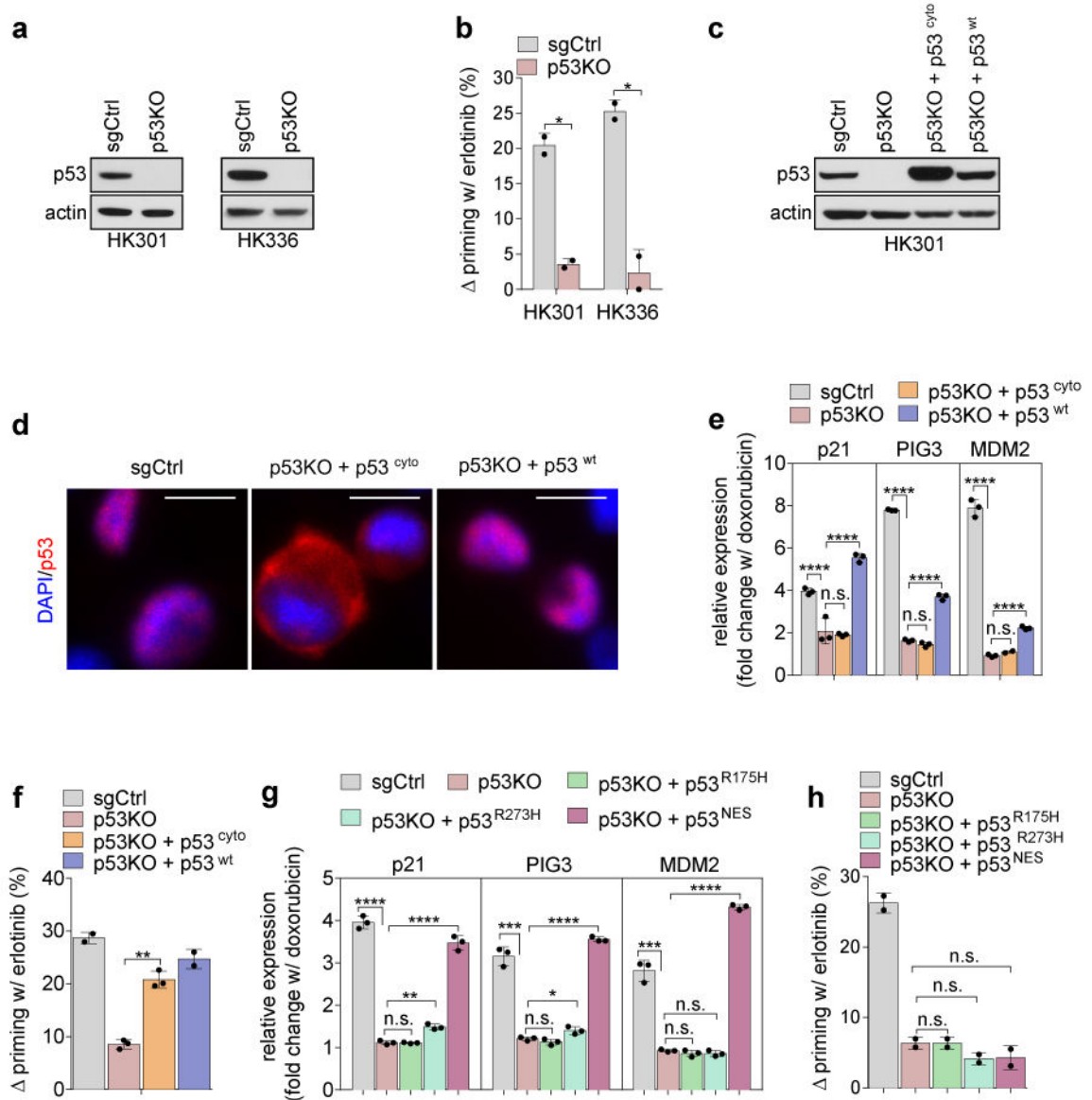
Figure 2. Cytoplasmic p53 links EGFR to intrinsic apoptosis
(a) Immunoblot of indicated proteins in two responders (HK301 and HK336) expressing CRISPR/CAS9 protein with control guide RNA (sgCtrl) or p53 guide RNA (p53KO). (b) The % change, relative to vehicle control, in apoptotic priming as determined by cytochrome *c* release following dynamic BH3 profiling with BIM peptides in sgCtrl and p53KO cells treated with 1 μM erlotinib for 24 hours (mean ± s.d., *n* = 2). BIM was selected based on exhibiting the greatest dynamic range from tested synthetic BH3 peptides (Supplemental Fig. 4). Results are representative of two independent experiments. (c) Immunoblot of indicated proteins in HK301 sgCtrl, p53KO, p53KO + p53^{cyto}, and p53KO + p53^{wt}. (d) Immunofluorescence of p53 protein combined with DAPI staining to reveal protein localization in HK301 sgCtrl, p53KO + p53^{cyto}, and p53KO + p53^{wt} (scale bars = 20 μm). (e) Changes in indicated mRNA levels following 100 nM doxorubicin treatment for 24 hours in HK301 sgCtrl, p53KO, p53KO + p53^{cyto}, and p53KO + p53^{wt}. Levels were normalized to

respective DMSO treated cells (mean ± s.d., $n = 3$). **(f)** Same as (b) but in HK301 sgCtrl, p53KO, p53KO + p53^{cyto}, and p53KO + p53^{wt} (mean ± s.d., $n = 2$). Results are representative of two independent experiments. **(g)** Same as (e) but in HK301 sgCtrl, p53KO, p53KO + p53^{R175H}, p53KO + p53^{R273H}, and p53KO + p53^{NES} (mean ± s.d., $n = 3$). **(h)** Same as (b) and (f) but in HK301 sgCtrl, p53KO, p53KO + p53^{R175H}, p53KO + p53^{R273H}, and p53KO + p53^{NES} (mean ± s.d., $n = 2$). Results are representative of two independent experiments. Comparisons were made using two-tailed unpaired Student's t-test. *p<0.05, **p<0.01, ***p<0.001, ****p<0.0001.
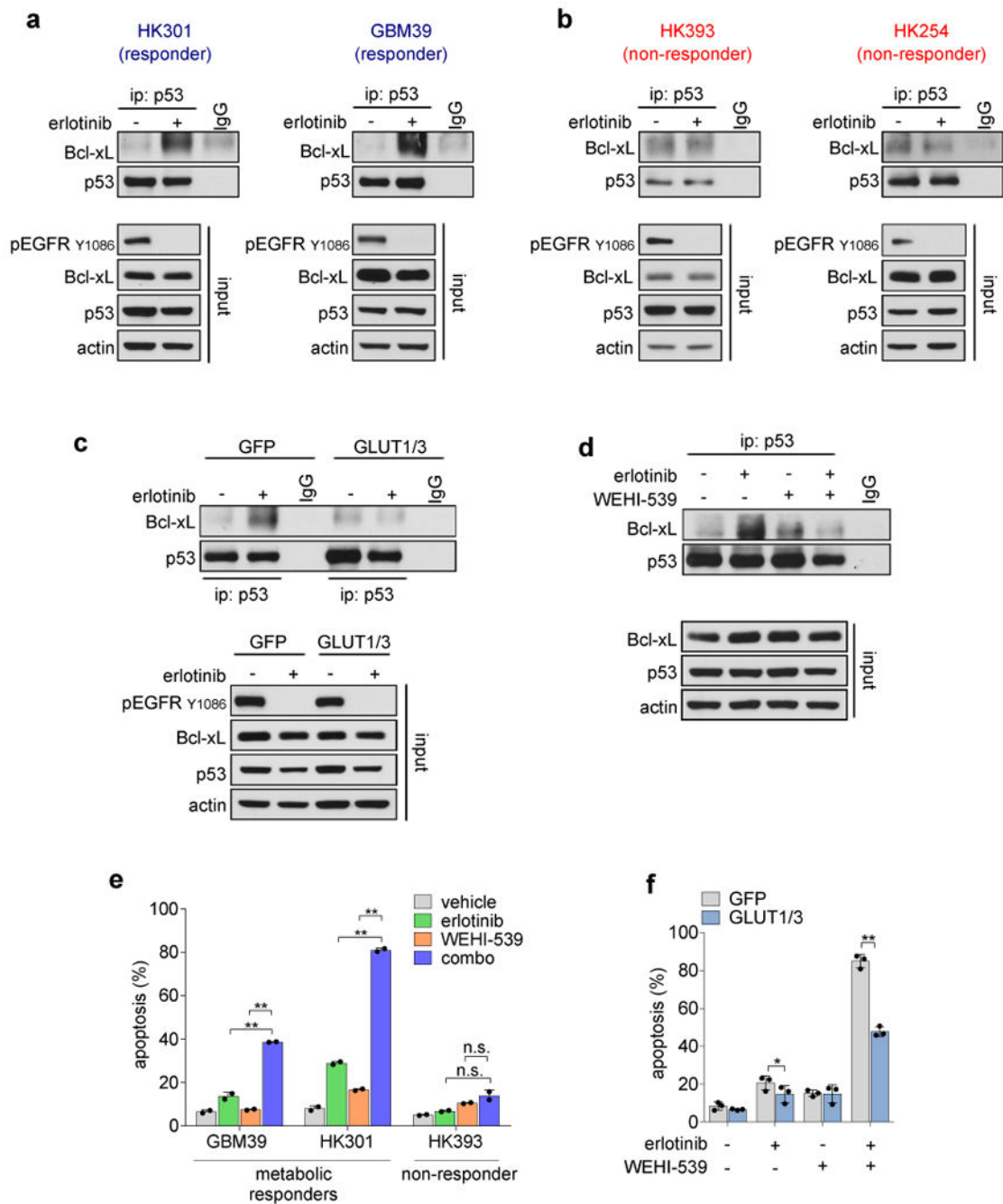
Figure 3. Bcl-xL prevents GBM cell death by binding to and sequestering cytoplasmic p53
(a) Immunoprecipitation of p53 in two metabolic responders (HK301 and GBM39) following 24 hours of 1 μM erlotinib treatment. Immunoprecipitation was performed with immunoglobulin G control antibody or anti-p53 antibody, and the immunoprecipitate was probed with the indicated antibodies. Below are respective pre-immunoprecipitation lysates (input). **(b)** Same as (a) but in two non-responders (HK393 and HK254). **(c)** Same as (a) and (b) but in HK301-GFP and HK301-GLUT1/3. **(d)** HK301 was treated for 24 hours with 1 μM erlotinib, 1 μM WEHI-539, or both and immunoprecipitation and immunoblotting was

performed as described previously. **(e)** Annexin V staining of two responders (GBM39 and HK301) and a non-responder (HK393) following 72 hours of treatment with 1 μM erlotinib, 5 μM WEHI-539, or both (mean ± s.d., $n = 2$). **(f)** Annexin V staining of HK301-GFP and HK301-GLUT1/3 following 72 hours of treatment with 1 μM erlotinib, 5 μM wehi-539, or both (mean ± s.d., $n = 2$). All results are representative of two individual experiments. Comparisons were made using two-tailed unpaired Student's t-test. *$p<0.05$, **$p<0.01$.
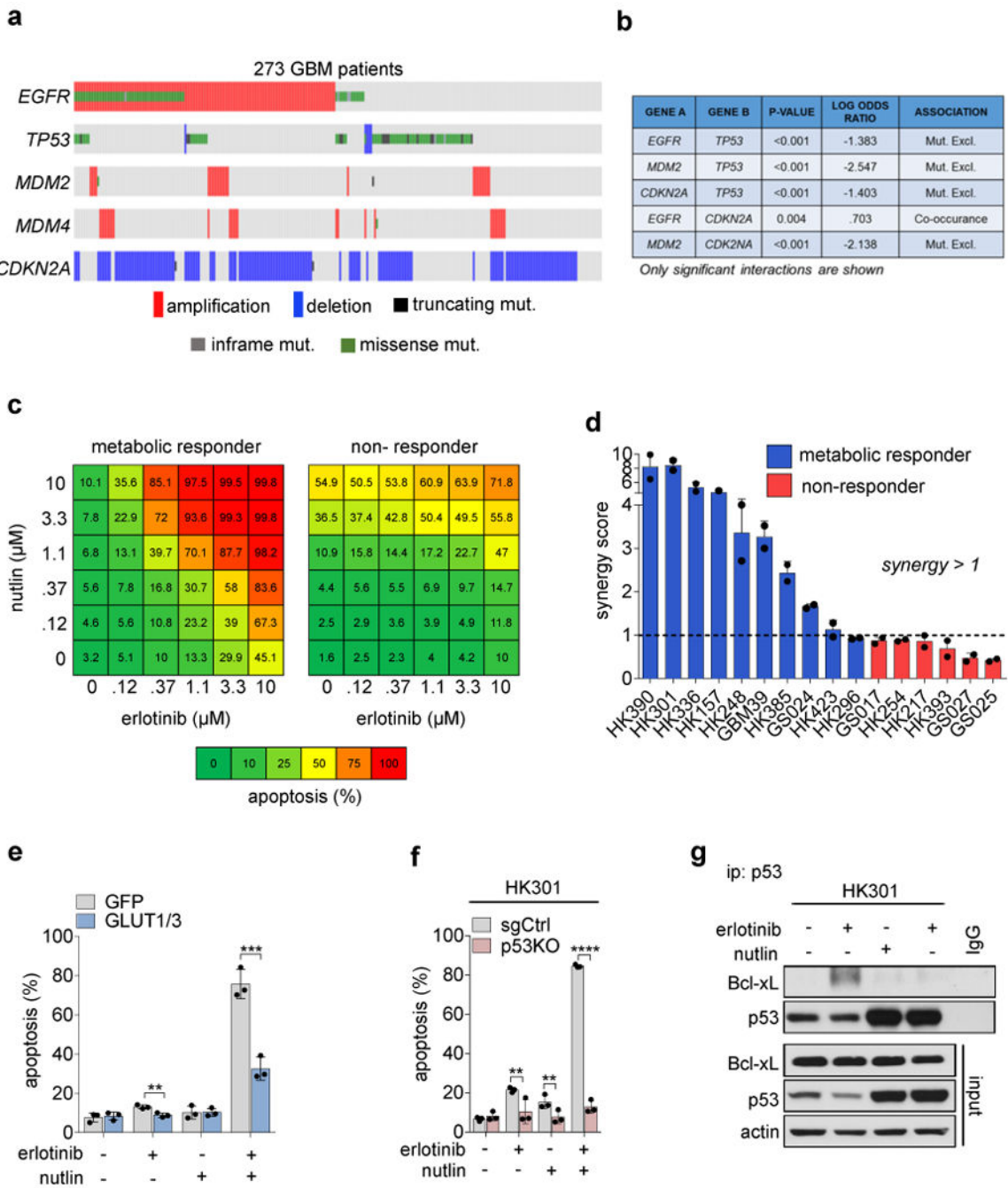
Figure 4. Synthetic lethality with combined targeting of EGFR and p53
(**a**) Summary of alterations in *EGFR* and genes involved in p53 regulation across 273 GBM samples. (**b**) Table indicating the significant associations between alterations in *EGFR* and genes involved in the p53 pathway. (**c**) Annexin V staining of a metabolic responder (left: HK301) and non-responder (right: HK393) treated with varying concentrations of erlotinib, nutlin, and in combination represented as a 6 × 6 dose-titration matrix. (**d**) The dose-titration of erlotinib and nutlin as described in (c) was conducted across 10 metabolic responders and 6 non-responders (all p53 wild-type), and the synergy score was calculated (see Materials

and Methods) (mean ± s.d., $n = 2$). Results are representative of two independent experiments. **(e)** Annexin V staining of HK301-GFP and HK301 GLUT1/3 following 72 hours of treatment with 1 μM erlotinib, 2.5 μM nutlin, or both (mean ± s.d., $n = 3$). Results are representative of two independent experiments. **(f)** Same as (e) but in HK301-sgCtrl and HK301 p53KO (mean ± s.d., $n = 3$). Results are representative of two independent experiments. **(g)** HK301 was treated for 24 hours with 1 μM erlotinib, 2.5 μM nutlin, or in combination. Immunoprecipitation was performed with immunoglobulin G control antibody or anti-p53 antibody, and the immunoprecipitate was probed with the indicated antibodies. Below are respective pre-immunoprecipitation lysates (input). Comparisons were made using two-tailed unpaired Student's *t*-test. ** p<0.01, *** p<0.001, **** p<0.0001
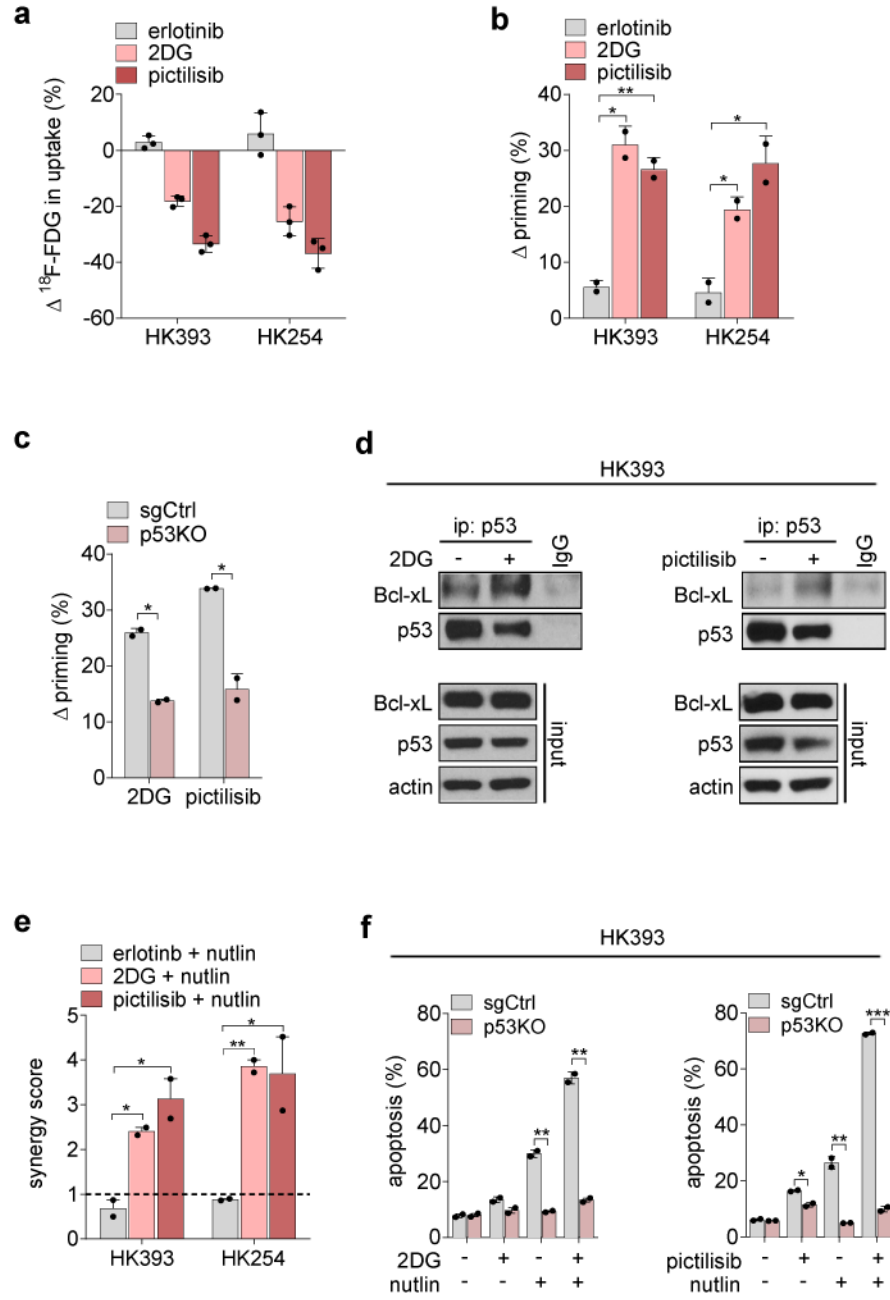
Figure 5. Modulation of glucose metabolism primes GBM for p53-mediated cell death
(a) % change in ^{18}F-FDG uptake after 4 hours of 1 μM erlotinib, 1 mM 2DG, or 1 μM pictilisib treatment relative to vehicle in HK393 and HK254 (mean ± s.d., $n = 3$). (b) The % change, relative to vehicle control, in apoptotic priming as determined by cytochrome c release following dynamic BH3 profiling using BIM peptides in HK393 and HK254 following 1 μM erlotinib, 1 mM 2DG, or 1 μM pictilisib for 24 hours (mean ± s.d., $n = 2$). Results are representative of two independent experiments (c) Same as (b) but in HK393 sgCtrl and p53KO (mean ± s.d., $n = 2$). (d) Immunoprecipitation of p53 in HK393 and HK254 following 24 hours of 1 mM 2DG or 1 μM pictilisib treatment. Immunoprecipitation

was performed with immunoglobulin G control antibody or anti-p53 antibody, and the immunoprecipitate was probed with the indicated antibodies. Below are respective pre-immunoprecipitation lysates (input). **(e)** Synergy score of various drugs (erlotinib, 2DG, and pictilisib) in combination with nutlin in HK393 and HK254 (mean ± s.d., $n = 2$). Results are representative of two independent experiments. **(f)** Annexin V staining of HK393 sgCtrl and HK393 p53KO following 72 hours of treatment with 0.5 mM 2DG, 1 μM pictilisib, 1 μM nutlin, 2DG + nutlin, or pictilisib + nutlin. (mean ± s.d., $n = 2$). Results are representative of two nindependent experiments. Comparisons were made using two-tailed unpaired Student's t-test. *p<0.05, **p<0.01, ***p<0.001.
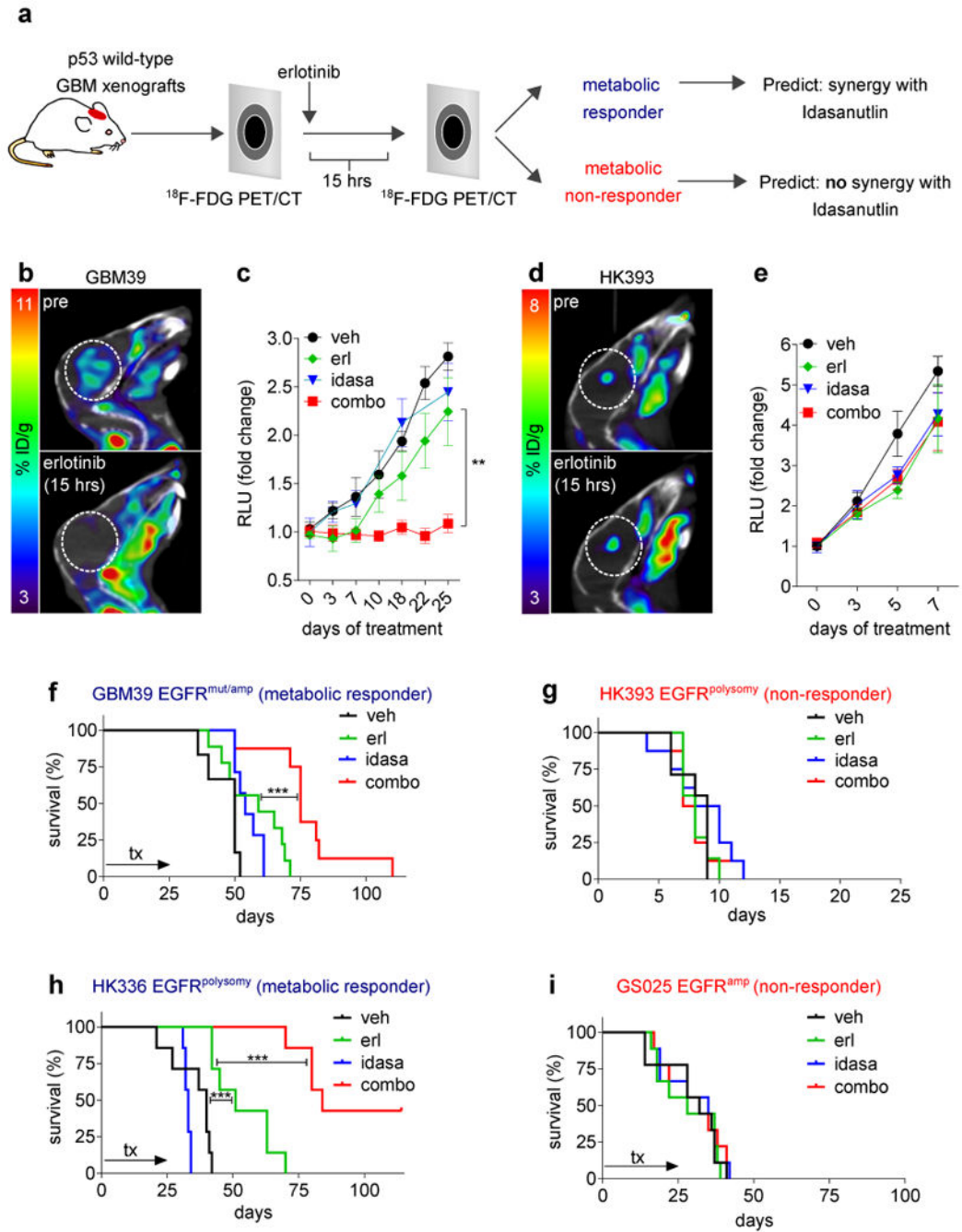
Figure 6. Combined targeting of EGFR-driven glucose uptake and p53 suppresses tumor growth *in vivo*

(**a**) Schematic of approach to use ^{18}F-FDG PET to rapidly predict changes in glucose uptake with EGFRi and consequently sensitivity to p53 stabilization with Idasanutlin. (**b**) Representative ^{18}F-FDG PET/CT images of GBM39 intracranial xenografts scanned before and after 15 hours of 75 mg/kg erlotinib treatment ($n = 3$ mice). (**c**) GBM39 intracranial xenografts were treated with vehicle ($n = 6$), 75 mg/kg erlotinib ($n = 9$), 50 mg/kg Idasanutlin ($n = 7$), or in combination daily ($n = 8$), and tumor burden was assessed at

indicated days using secreted *gaussia* luciferase (mean ± s.d.) (see Materials and Methods for *gaussia* luciferase measurements). **(d)** Same as (b) but in HK393 intracranial xenografts. **(e)** Same as (c) but in HK393 intracranial xenografts (mean ± s.d., $n = 7$ for all groups). **(f)** % survival of (c). **(g)** % survival of (e). **(h)** % survival of metabolic responder HK336 following indicated treatments for 25 days and then released from drug ($n = 7$ for all groups). **(i)** % survival of non-responder GS025 following indicated treatments for 25 days and then released from drug ($n = 9$ for all groups). Comparisons for (c) and (e) used data sets from the last measurements and were made using two-tailed unpaired *t*-test. Kaplan–Meier survival analysis (log-rank) was used for (f) – (i). **p <0.01, ***p<0.001.